Molecular Dynamics Simulations of the Tau Amyloid Fibril Core Dimer at the Surface of a Lipid Bilayer Model: I. In Alzheimer's disease

Phuong H Nguyen, Philippe Derreumaux

Molecular Dynamics Simulations of the Tau Amyloid Fibril Core Dimer at the Surface of a Lipid Bilayer Model: I. In Alzheimer's disease

Phuong H Nguyen,[1] and Philippe Derreumaux [1,2*]

1 CNRS, Université Paris Cité, UPR 9080, Laboratoire de Biochimie Théorique, Institut de Biologie Physico-Chimique, Fondation Edmond de Rothschild, 13 rue Pierre et Marie Curie, 75005 Paris, France.

2 Institut Universitaire de France (IUF)

ABSTRACT

The tau R3-R4 domain spanning residues 306-378 was shown to form the amyloid fibril core of full-length tau in the brain of patient with Alzheimer's disease. Recently, we studied the dynamics of tau R3-R4 monomer at the surface of a lipid bilayer model and revealed deep insertion of the amino acids spanning the PHF6 motif (residues 306-311) and its flanking residues. Here, we explore the membrane-associated conformational ensemble of tau R3-R4 dimer by means of atomistic molecular dynamics. Similar to the monomer simulation, R3-R4 dimer has the propensity to form β-hairpin-like conformation. Unlike the monomer, the dimer shows deep insertion of the C-terminal R4 region and transient adsorption of the PHF6 motif. Taken together, these results reveal the multiplicity of adsorption and insertion modes of tau into membranes depending on its oligomer size.

INTRODUCTION

Tauopathies leading to 20 neurodegenerative diseases are characterized by the aggregation of the intrinsically disordered protein (IDP) tau in neurons and glia.[1-4] Full-length tau encoding 441 amino acids consists of a projection N-terminal domain, a microtubule-binding domain of four repeats (labeled R1−R4), and a basic C-terminal. In Alzheimer's disease (AD), the neurological hallmarks are the formation of neurofibrillary tangles (NFTs), neuropil threads and dystrophic neurites in neocortex and limbic regions.[1] In Pick's disease (PiD), the neurological hallmarks are the formation of cytoplasmic spherical structures, termed Pick Bodies, in frontal, temporal, and parietal lobes.[2] Other tauopathies include chronic traumatic encephalopathy, corticobasal degeneration and progressive supranuclear palsy.[3,4]

As evidenced by cryo-electron microscopy (cryo-EM), the N-terminal 305 and C-terminal 62 residues of full-length tau are flexible and disordered in the fibrils isolated from the brain of an individual with AD.[5] Using the same structural technique, the N-terminal 253 residues and C-terminal 62 residues of full-length tau are disordered in the fibrils isolated from the brain of patients suffering from Pick's disease (PiD).[6] The two structures of tau are therefore linked to different forms of dementia,[7] and a structure (filament fold)-based classification of tauopathies was recently reported.[8]

The amyloid fibril core of tau in AD spans the R3-R4 domain (residues 306-378) with a C-shaped architecture consisting of eight β-strands and a β-helix motif spanning residues 336-354.[5] The amyloid fibril core of tau in PiD spans the R1-R3-R4 domain, residues 254-378 lacking therefore the second microtubule-binding repeat spanning residues 275-305 in the numbering of the 441 amino acid human tau isoform. In contrast to AD fold, PiD fold has an elongated architecture consisting of nine β-strands arranged into four cross-β packing stacks connected by turns and arcs.[6] Apart from a difference in filament folds, the hexapeptide called PHF6 (VQIVYK, residues 306−311 in R3), which is essential for tau amyloid formation,[9] locks into the HKLTF sequence (residues 374-378) in AD fibril, while it locks into the QVEVK sequence (residues 336-340) in PiD fibril.[10]

It was demonstrated that tau oligomers are highly toxic *in vitro* due their capacity to act as a seed in the misfolding and propagation of AD pathology.[11] Tau oligomers can self-assemble into amyloid fibrils in the bulk solution in the presence of polyanions, and at the surface of membrane models.[12,13] It is well established that the morphology and filament fold vary with cofactors.[14,15] The accumulation of oligomers on membrane surfaces can remodel and disrupt membranes, extracts lipids, and all these effects are regulated by the membrane composition and proteins concentration.[16-18]

Among the low molecular weight aggregates, tau dimers are particularly important in AD pathology. Their formation appear to be the rate-limiting step of tau aggregation *in vitro*.[19] Dimers are also observed in cells[29] and in the cerebrospinal fluid of AD patients.[21] Curcumin suppresses soluble dimers and corrects behavioral deficits in aged human tau transgenic mice.[22] The size, flexibility, disorder and transient characters of dimers have prevented structure determination by NMR spectroscopy.

We recently explored the conformations of tau R3-R4 domain monomer in the bulk solution and at the surface of a lipid bilayer model,[23] and of tau R3-R4 domain dimer in the bulk solution.[24] Studying the R3-R4 sequence as a model of the full-length sequence is justified as tau297-391 spontaneously forms fibrils under physiological conditions similar to those found in AD brain tissues.[25] The atomistic molecular dynamics (MD) simulations in the bulk solution revealed (a) R3-R4 turn/coil monomers with a small propensity to form transient β-hairpins in compact and expanded forms[23]; and (b) R3-R4 dimers with elongated, U-shaped, V-shaped and globular forms rather than the C-shaped form observed in AD fibrils.[24] MD simulations of R3-R4 monomer at the surface of a DOPC/DOPS bilayer membrane showed a conformational ensemble markedly different from that in the bulk solution and revealed the dynamical properties of the membrane-bound state of tau R3-R4 monomer enabling insertion of the residues 306-318 and 376-378.[23]

Given the high importance of tau dimers in AD pathology, and as a first step towards elucidating the link between different amyloid forms and distinct dementia, here we report on the early binding steps at an atomistic level of tau R3-R4 dimer at the surface of a DOPC/DOPS lipid membrane by means of two MD simulations starting from distinct structures. A few

simulations using atomistic and coarse-grained models explored the conformational ensemble of tau monomers going beyond one single repeat in the bulk solution,[26-32] to understand in particular the impact of disease-mutations at residue P301,[31] and whether the liquid-liquid phase separation of tau R1-R4 domain is encoded in monomer.[32] However, no molecular simulations and NMR studies were conducted to study the interactions of the R3-R4 dimer with lipid membranes.

MATERIALS and METHODS

MD simulations were performed using the GROMACS package[33] with the CHARMM36 protein field and the TIP3P water model.[34] Although CHARMM36m was found to work better on a few IDPs in the bulk solution,[35] its performance on amyloid peptide-membrane systems remains to be determined. Tau is capped by acetyl and amide at N- and C-termini, and at pH 7, the peptide has neutral His with a protonated Nε atom, protonated Arg and Lys and deprotonated Glu and Asp. Two starting conformations were used; the cryo-EM fibril structure[5] and one globular compact structure which has a probability of 20% in a previous replica exchange molecular dynamics study in the bulk solution.[24]

The tau structures were positioned at a distance of 1.4 nm from the bilayer surface. Both the cryo-EM and globular structures were set parallel to the membrane surface. The bilayer consisting of 320 DOPC and 320 DOPS lipids was immerged in a box of (15.1, 15.1 and 9.2 nm) containing 33530 water molecules. Each tau system was neutralized by sodium ions leading to a total number of about 189000 atoms. CHARMM-GUI was used to set up the system.[36]

Each system was minimized with harmonic restraints on the backbone atoms, and then equilibrated with restraints by MD for 1 ns in the NVT ensemble and 1 ns in the NPT ensemble. Van der Waals interactions were truncated at 1.1 nm, and the electrostatic interactions were calculated using the particle mesh Ewald method using a cutoff of 1.2 nm. MD simulations were carried out on each system for 2 μs at 303 K in the NPT ensemble with a timestep of 2 fs using the LINCS algorithm[33] and the velocity-rescaling thermostat.[37]

Figure 1A-B show the two initial structures after equilibration. The cryo-EM structure features eight β-strands or sheets encompassing residues V306-K311 (strand β1), V313-C322 (β2), N327-K331 (β3), Q336-S341 (β4), K343-K347 (β5), R349-I354 (β6), S356-V363 (β7) and N368-F378 (β8). The globular structure features seven native β-strands or sheets. The main secondary structure difference with the cryo-EM structure is the absence of β7 strand, and the breaking of the 11-residue β8-strand into two strands encompassing residues N368-E372, and K375-L377.

Secondary structures were determined using the DSSP method.[38] The two trajectories were combined and projected on the first two principal components obtained after diagonalization of the positional fluctuation covariance matrix of the backbone peptides.[39] The 2D free energy landscape was constructed using the formula $-RT \times \log(H(x,y))$, where H(x,y) is the histogram of the parameters x and y.[40] The number of clusters, the center and the population of each cluster were determined using k-means algorithm.[41,42]

Conformations were also characterized by their radii of gyration (Rg), Cα end-to-end distances and specific intermolecular Cα distances averaged over the two chains and their contact map probabilities. A contact between two side-chains was formed if there is at least one distance smaller than 0.45 nm between all heavy atoms. We counted all contacts between a side-chain and the lipid (head, glycerol, hydrophobic tail1 and hydrophobic tail2) groups when the distance between heavy atoms is smaller than 0.45 nm. We also considered all heavy atom contacts between the backbone of each residue and lipid components within a cutoff of 0.45 nm.

RESULTS and DISCUSSION

Our goal is to understand the early misfolding and binding steps of tau R3-R4 dimer at the surface of a lipid bilayer model. Capturing the equilibrium ensemble of tau dimer/membrane is out of reach using atomistic models and explicit solvent and membrane environments. The distributions of the radius of gyration (Figure 2A) and of the Cα end-to-end distance (Figure 2B) reveal that the trajectory from the globular structure explores a limited conformational space, the Rg peak being centered at 1.7 nm and varying between 1.5 and 2 nm and the end-to-end

distance varying between 0.8 and 1.5 nm. Starting from the cryo-EM structure, the Rg distribution varies between 1.8 and 2.7 nm, and the end-to-end distance distribution shows three peaks at 1.1, 1.4 and 2.6 nm with a tail up to 4 nm. The two simulations lead therefore to two distinct conformational ensembles within 2 μs.

Their secondary structure contents do not differ substantially, however. The (β, helix, coil and turn) contents amount to (28.3, 0.4, 17.6 and 53.6%) from the cryo-EM structure and (19.0, 0.4, 24.1 and 56.4%) from the globular structure, with standard errors using distinct time windows of ± 3% for β, coil and turn contents. Both simulations give therefore values that vary markedly from the fibril content of (57.5, 0.0, 34.3, 8.0%). Differences between the two simulations are evidenced by the β, helix, coil and turn contents along the sequence shown in Figure S1 (see Supporting Information). Only, the PHF6 region (residues V306-K311) maintains a very strong β-sheet signal in both simulations with an average value of 60%. The cryo-EM simulation retains high β-sheet signal in three other regions spanning residues N327-H330, S356-H362 and N369-L376. In this simulation, the residues V313-G326, K331-Q351 and V363-N368 have strong coil and turn characters. The second simulation keeps high β-strand character for the residues V337-V339, V350, E370 and D377.

The β, helix, coil and turn contents along the sequence averaged over the two simulations are shown in Figure 3. Four fibril β-sheet regions are maintained among a total of eight and encompass the β1, β3, β4 and β8 regions. This is also reflected by the intermolecular side chain contact map shown in Figure 4A with the highest probabilities (> 50%) involving the β1-β1, β3-β3, β4-β4 and β8-β8 amino acids. In contrast, the β2, β5, β6 and β7 regions are dominated by turn and coil (Figure 3).

Overall, the surface of the membrane reduces the β-sheet signal compared to tau dimer in the bulk solution, where all β regions have a β-strand propensity > 40% (see Figure 3 in Ref. 24). This result is in agreement with MD simulations of tau306-378 monomer[23] and Aβ42 dimer[43] interacting with membrane model. The PHF6 region is found to have the highest β-sheet content along the region 306-378 when tau is adsorbed on the membrane surface.

The role of the PHF6 motif to drive tau fibril formation in the bulk solution was discussed many times.[4,9] Our simulations show that the PHF6 propensity for parallel β-sheet is slightly higher in the presence of membrane (60%) than in aqueous solution (50%), and compared to the tau306-378 monomer-membrane simulation, dimerization of tau at the membrane increases the β-sheet signal from 9.5% to 24%. This is consistent with *in vitro* experiments showing an enhanced tau nucleation and fibrillation kinetics at the membrane compared to the bulk solution.[12,18] Our dimer simulations do not reveal α-helix signal. This suggests that, although regions of R3 fold into α-helices upon binding to membranes,[12] the transition from α-helix to β-sheet structure may occur during the very early stages of dimerization which are not captured by our simulations.

The conservation of the N- and C-terminal β-sheets suggests a very sparse intramolecular side chain contact map. As seen in Figure 4B, the number of contact pairs separated by at least four residues with a probability > 40% is very small: one long-range contact between residues I354 and V337 (probability of 62%), and one short-range contact between residues L344 and V339 (probability of 44%), both contacts being located in the β-helix region. Figure 4B also reports on few short-lived side chain interactions with a probability varying between 10 and 30% distributed over the full map reflecting the intrinsic disorder and limited flexibility of each chain within the dimer.

The conformational ensemble of tau306-378 dimer is further investigated by the FEL using the combined MD trajectories to compute the first two principal components V1 and V2 (Figure 5). Eight minima, designated as Si and covering three distinct (V1, V2) subspaces, are identified. The structures of the center of each cluster are shown in Figure 6. The secondary structural characteristics and population of each cluster, and the total number of side-chain contacts with the membrane are given in Table S1 in the Supporting Information.

The first class of conformations, consisting of S1 (population of 21.4%), S4 (13.9%), S5 (11.8%) and S8 (3%) clusters with an averaged Rg of 1.6 nm, includes compact globular shapes (Table S1). Clusters S1, S4 and S5 have an averaged β content of 19%. S1 is characterized by three parallel intermolecular β-sheets spanning residues Q307-V309 (PHF6), V337-V339 and L376-T377, Q307-V309 sheet being antiparallel to V337-V339 sheet, L376-T377 β-sheet being

perpendicular to L376-T377 β-sheet, and the rest of the amino acids being turn/coil (80%). Clusters S4 and S5 display a four-stranded parallel β-sheet spanning residues Q307-Y310 (PHF6) and V337-V339 with the two C-termini forming transient hydrogen-bonding interactions. The center of the cluster S8 with the highest β content (28%) among the globular shapes maintains the parallel PHF6 (Q307-Y310) β1-sheet and β8-sheet (K369-L376), and parts of the β2-sheet (residues V313-D314 and L317-V318), β3-sheet (H329-H330) and β6-sheet (V350-I354).

The second class of conformations consists of U-shaped (S6, population of 11%) and elongated (S2, 20.5%; S3, 14% and S7, 4.5%) topologies. The elongated forms differ in β-sheet compositions and positions. Cluster S7 consists of a parallel β-sheet spanning PHF6 motif (Q307-V309), a β-hairpin spanning residues I328-P332 and N359-H62 in one chain forming parallel hydrogen-bonding interactions with residues I328-H330 of the other chain, and the two C-termini disjointed (distance of 5 nm). Cluster S3 maintains the PHF6 β1- (residues Q307-V309) and β8- (residues I371-L376) sheets, and has a much less curved loop region than in the cryo-EM structure as a result of the formation of a β-hairpin spanning residues H329-P332 and K353-L357 in one chain. Cluster S2 is topologically similar to S3, the exception being the large end-to-end distance between the two C-termini (3.6 nm), and the presence of a loop region between the PHF6 motif and the residues than span the β2-sheet in the cryo-EM structure. Cluster S6, with a U-shaped topology, displays six β-sheets (β1 to β4, β7 and β8 regions) with shorter lengths than in the cryo-EM structure, and a change of the orientation of the β-helix region pointing outward rather than inward.

Overall, because the simulation from the compact structure captures clusters S1, S4, S5 and S8 clusters, and that from the cryo-EM structure captures clusters S2, S3, S6 and S7, longer simulations times are required to observe transitions between the topologies. Based on the present results, the lifetime of aggregates with many distinct states is at least of 2 microseconds. Like the dimer simulation in the bulk solution, tau306-378 has a high propensity to form elongated, U-shaped, and globular architectures at the membrane surface, and has a very negligible probability to form the C-shaped cryo-EM topology. Tau306-378 dimer has also a non-negligible propensity to form β-hairpin-like monomers. β-hairpins were discussed in amyloid-β fibril formation in pure buffer,[4] and at the surface of membranes.[43] The membrane-associated

aggregation of human islet amyloid polypeptide (hIAPP) was also found to proceed by assembling β-hairpin-like monomers at the lipid bilayer surface.[44]

Concomitantly with different topological features upon membrane binding, the interactions of tau306-376 with the lipid bilayer are highly dynamic and diverse. There is no clear separation in the total number of side chain contacts with the membrane between the clusters, the exception being the U-shaped topology with an average of 100 contacts (Table S1). The number of contacts tends however to be higher for the globular shapes than for the elongated shapes; this number varying between 204 and 634 for the conformations starting from the cryo-EM structure, and between 481 and 685 starting from the globular structure. But heterogeneity is observed in each class of conformations, the two elongated S2 and S3 structures having 634 and 224 contacts, respectively.

The total number of contact pairs between the side chain of each residue and each lipid component (head, glycerol, tail1 and tail2) is analyzed into the two groups of simulations (Figure 7). Our initial expectations based on the R3-R4 monomer simulation were that the PHF6 motif would adhere well to the membrane. We also anticipated that insertion of tau would be driven by the side chains of PHF6 motif and its flanking residues P312-V318. It is therefore surprising that the R4 domain and in particular residues L344-S352 and I360-F378, and not the PHF6 motif, interact strongly with the head and glycerol lipid groups in both simulations. Of note, residue R349 shows more contacts from the compact simulation than from the cryo-EM simulation (about 30 vs. 10 contacts). Compact topologies tend to interact with the membrane through residues I360-V371 and to a lesser extent residues K317-K331, whereas elongated topologies tend to interact with membrane through residues N368-F378 and to a lesser extent residues K317-K331. The residues I360-F378 have a higher propensity than residues L344-Q351 to insert more deeply into the membrane, the number of contacts remains however small with tail1 group (on average 3 contacts per residue) and very small with tail2 group (on average 1 contact per residue). Insertion of tau dimer is therefore much less pronounced that for tau monomer, where the number of contacts between PHF6 side chains and (tail1, tail2) groups reached (30, 10) contacts for V306 (see Figure 8 in Ref. 23). Figure 1C-D show the MD-generated structures at 2 μs from the two simulations.

To explore the possibility that PHF6 could make very short-lived contacts with the lipid components and characterize the dynamics of tau dimer, we followed the time-evolution of several parameters starting from cryo-EM structure. These variables include the β-strand content of PHF6 and the full sequence (Figure S2A in the Supporting Information), the intermolecular Cα F378-F378 distance (Figure S2B), and the total number of contacts (including both backbone and side chain heavy atoms) between each residue of PHF6 with the lipid head and glycerol groups (Figures S3 and S4 in the Supporting Information).

During the first microsecond, the β-sheet of the full sequence decreases continuously to an average value of 25% while maintaining a PHF6 β-sheet content between 37.5 and 65% (Figure S2A), and the intermolecular F378-F378 contact remains formed (Figure S2B). Subsequently, the β-sheet of PHF6 and the full sequence fluctuates between 37.5 and 50%, and between 15 and 35%, respectively and the two C-termini detach from each other, the intermolecular Cα F378-F378 distance fluctuating between 2 and 7 nm. Conjointly, we observe transient contacts of the PHF6 residues of both chains with the head groups of lipids. Binding is highly dynamic with a succession of adsorption and de-absorption events, with almost no binding from 500 to 900 ns and 1200 to 1600 ns (Figure S3). Contacts of PHF6 residues with the glycerol lipid groups are relatively rare during the full simulation (Figure S4). These results indicate transient adsorption of the PHF6 residues on the membrane by backbone and side-chain interactions.

CONCLUSIONS

In summary, we have reported on the membrane-associated conformational ensemble of tau306-378 dimer at an atomistic level by a series of MD simulations (microseconds). Such long MD simulations from two distinct starting conformations can reveal the potential membrane insertion modes and may explain tau-induced toxicity.

When adsorbed on the membrane, the dimer remains mostly in a random coil state. Of note however the β-sheet content of the PHF6 motif (residues V306-K311) is very high, and dimerization of tau at the membrane increases significantly the β-sheet signal compared to the tau monomer-membrane system. Simulations reveal that the membrane does not stabilize the

C-shaped cryo-EM state, and the dimer has a non-negligible propensity for β-hairpin like monomers. This β-hairpin was observed for the aggregation of amyloid-β[43] and hIAPP[44] peptides at the surface of bilayer membranes.

The early binding steps reveal that dimerization has a considerable impact on the insertion modes. While the monomer simulation revealed deep insertion of the amino acids spanning the PHF6 motif (residues V306-K311) and its flanking residues (up to V318) into the membrane, all residues being random coil, the dimer simulation points to transient adsorption of the residues V306-V318 and strong insertion of residues L344-S352 and I360-F378 into the membrane. Taken together, our monomer and dimer simulations provide a complex mechanistic view on how tau can extract phospholipids from the membrane,[17,45] explaining therefore the formation of toxic tau/phospholipid oligomers,[17] and the presence of various phospholipids in brain derived tau filaments.[46]

To which extent our results can be extrapolated to full-length tau and *in vivo* conditions remains to be determined. Integrating the R2 repeat and the PHF6* motif (residues V275-K280 at the start of R2) is important as they are known to interact with negatively charged vesicles.[17] The PHF6* motif is also aggregation-prone,[4] and may form metastable compact structures with its upstream sequence that modulates aggregation propensity.[47] Complexifying membrane composition[43,48,49] and exploring phosphorylation at given sites[4] are also two important issues to explore in order to develop more efficient drugs.[4,50-52]

ASSOCIATED CONTENT

Supporting Information

The Supporting Information is available free on charges on the ACS Publications website at DOI:

Additional results: Secondary structure compositions along the amino acid sequence starting from the cryo-EM and compact structures; structural characterization of the centroids; time-evolution of β-strand of the PHF6 motif and the full sequence; time-evolution of side-chain and backbone contacts between the PHF6 residues and the head and glycerol lipids. (PDF)

AUTHOR INFORMATION

Corresponding Author

*E-mail: philippe.derreumaux@ibpc.fr

ORCID

Phuong H. Nguyen: 0000-0003-1284-967X

Philippe Derreumaux: 0000-0001-9110-5585

Notes

The authors declare no competing financial interest.

ACKNOWLEDGMENTS

This work was supported by grants from the French IDRIS and CINES computer centers, and the "Initiative d'Excellence" program from the French State, Grant "DYNAMO", ANR-11-LABX-0011.

REFERENCES

1. Perry, G.; Kawai, M.; Tabaton, M.; Onorato, M.; Mulvihill, P.; Richey, P.; Morandi, A.; Connolly, J.A.; Gambetti P. Neuropil Threads of Alzheimer's Disease show a Marked Alteration of the Normal Cytoskeleton. *J Neurosci.* **1991,** *11*, 1748-1755.
2. Lee, V.M.; Goedert, M.; Trojanowski, J.Q. Neurodegenerative Tauopathies. *Annu. Rev. Neurosci.* **2001**, *24*, 1121–1159.
3. Silva, M.C.; Haggarty, S.J. Tauopathies: Deciphering Disease Mechanisms to Develop Effective Therapies*. Int J Mol Sci.* **2020**, *21*, 8948.
4. Nguyen, P.H.; Ramamoorthy, A.; Sahoo, B.R.; Zheng, J.; Faller, P.; Straub, J.E, Dominguez, L.; Shea, J.E.; Dokholyan, N.V.; De Simone, A. et al. Amyloid Oligomers: A Joint Experimental/Computational Perspective on Alzheimer's Disease, Parkinson's Disease, Type II Diabetes, and Amyotrophic Lateral Sclerosis*. Chem Rev* **2021**, *121*, 2545-2647.
5. Fitzpatrick, A. W. P.; Falcon, B.; He, S.; Murzin, A. G.; Murshudov, G.; Garringer, H.J.; Crowther, R.A.; Ghetti, B.; Goedert, M.; Scheres, S. H. W. Cryo-EM Structures of Tau Filaments from Alzheimer's Disease. *Nature* **2017**, *547*, 185−190.
6. Falcon, B.; Zhang, W.; Murzin, A.G.; Murshudov, G.; Garringer, H.J.; Vidal, R.; Crowther, R.A.; Ghetti, B.; Scheres, S.H.W; Goedert, M. Structures of Filaments from Pick's Disease Reveal a Novel Tau Protein Fold. *Nature.* **2018**, *561*, 137-140.
7. Goedert M.; Falcon, B.; Zhang, W.; Ghetti, B.; Scheres, S.H.W. Distinct Conformers of Assembled Tau in Alzheimer's and Pick's Diseases. *Cold Spring Harb Symp Quant Biol.* **2018**, *83,* 163-171.
8. Shi, Y.; Zhang, W.; Yang, Y.; Murzin, A.G.; Falcon, B.; Kotecha, A.; van Beers, M.; Tarutani, A.; Kametani, F.; Garringer, H.J. et al Structure-based Classification of Tauopathies. *Nature.* **2021***, 598*, 359-363.
9. von Bergen, M.; Friedhoff, P.; Biernat, J.; Heberle, J.; Mandelkow, E.M.; Mandelkow, E. Assembly of Tau Protein into Alzheimer Paired Helical Filaments Depends on a Local Sequence Motif ((306)VQIVYK(311)) Forming beta Structure. *Proc Natl Acad Sci U S A.* **2000**, *97*, 5129-5134.
10. Lippens, G.; Gigant, B. Elucidating Tau Function and Dysfunction in the Era of cryo-EM. *J Biol Chem.* **2019**, *294*, 9316-9325.

11. Jucker, M.; Walker, L.C. Self-propagation of Pathogenic Protein Aggregates in Neurodegenerative Diseases. *Nature*. **2013**, *501*, 45-51.
12. Sallaberry, C.A.; Voss, B.J.; Majewski, J.; Biernat, J.; Mandelkow, E.; Chi, E.Y.; Vander Zanden, C.M. Tau and Membranes: Interactions That Promote Folding and Condensation. *Front Cell Dev Biol.* **2021**, *9*, 725241.
13. Barré, P.; Eliezer, D. Structural Transitions in Tau k18 on Micelle Binding Suggest a Hierarchy in the Efficacy of Individual Microtubule-binding Repeats in Filament Nucleation. *Protein Sci.* **2013**, 22, 1037-1048.
14. Fichou, Y.; Vigers, M.; Goring, A.K.; Eschmann, N.A; Han, S. Heparin-induced Tau Filaments are Structurally Heterogeneous and Differ from Alzheimer's Disease Filaments. *Chem Commun (Camb).* **2018**, *54*, 4573-4576.
15. Abskharon, R.; Sawaya, M.R.; Boyer, D.R.; Cao, Q.; Nguyen, B.A.; Cascio, D.; Eisenberg, D.S. Cryo-EM Structure of RNA-induced Tau Fibrils Reveals a Small C-terminal Core that May Nucleate Fibril Formation. *Proc Natl Acad Sci U S A.* **2022**, *119*, e2119952119
16. Jones, E.M.; Dubey, M.; Camp, P.J.; Vernon, B.C.; Biernat, J.; Mandelkow, E.; Majewski, J.; Chi, E.Y. Interaction of Tau Protein with Model Lipid Membranes Induces Tau Structural Compaction and Membrane disruption. *Biochemistry.* **2012**, *51*, 2539-2550.
17. Ait-Bouziad, N.; Lv, G.; Mahul-Mellier, A.L.; Xiao, S.; Zorludemir, G.; Eliezer, D.; Walz, T.; Lashuel, H.A. Discovery and Characterization of Stable and Toxic Tau/phospholipid Oligomeric Complexes. *Nat. Commun.* **2017**, *8*, 1678.
18. Fanni, A.M.; Vander Zanden, C.M.; Majewska, P.V.; Majewski, J.; Chi, E.Y. Membrane-mediated Fibrillation and Toxicity of the Tau Hexapeptide PHF6. *J Biol Chem*. **2019**, *294*, 15304-15317.
19. Schweers, O.; Mandelkow, E.M.; Biernat, J.; Mandelkow, E. Oxidation of Cysteine-322 in the Repeat Domain of Microtubule-associated Protein Tau Controls the in vitro Assembly of Paired Helical Filaments. *Proc Natl Acad Sci U S A.* **1995**, *92*, 8463-8467.
20. Wegmann, S.; Nicholls, S.; Takeda, S.; Fan, Z.; Hyman, B.T. Formation, Release, and Internalization of Stable Tau Oligomers in Cells. *J Neurochem.* **2016**, *139*, 1163-1174.
21. Takeda, S.; Commins, C.; DeVos, S.L.; Nobuhara, C.K.; Wegmann, S.; Roe, A.D.; Costantino, I.; Fan, Z.; Nicholls, S.B.; Sherman, A.E. et al. Seed-competent High-molecular-weight Tau Species Accumulates in the Cerebrospinal Fluid of Alzheimer's Disease Mouse Model and Human Patients. *Ann Neurol.* **2016**, *80*, 355-367.
22. Ma, Q.L.; Zuo, X.; Yang, F.; Ubeda, O.J.; Gant, D.J.; Alaverdyan, M.; Teng, E.; Hu, S.; Chen, P.P.; Maiti, P et al. Curcumin Suppresses Soluble Tau Dimers and Corrects Molecular Chaperone, Synaptic, and Behavioral Deficits in Aged Human Tau Transgenic Mice. *J Biol Chem.* **2013,** *288,* 4056-4065.
23. Nguyen, P.H.; Derreumaux, P. Molecular Dynamics Simulations of the Tau R3-R4 Domain Monomer in the Bulk Solution and at the Surface of a Lipid Bilayer Model. *J Phys Chem B.* **2022**, xx, yy-zz.

24. Derreumaux, P.; Man, V.H.; Wang, J.; Nguyen, P.H. Tau R3-R4 Domain Dimer of the Wild Type and Phosphorylated Ser356 Sequences. I. In Solution by Atomistic Simulations. *J Phys Chem B.* **2020**, *124*, 2975-2983.
25. Al-Hilaly, Y.K.; Foster, B.E.; Biasetti, L.; Lutter, L.; Pollack, S.J.; Rickard, J.E.; Storey, J.M.D.; Harrington, C.R.; Xue, W.F.; Wischik, C.M. et al. Tau(297-391) Forms Filaments that Structurally Mimic the Core of Paired Helical Filaments in Alzheimer's Disease Brain. *FEBS Lett.* **2020**, *594*, 944-950.
26. Popov, K.I.; Makepeace, K.A.T.; Petrotchenko, E.V.; Dokholyan, N.V.; Borchers, C.H. Insight into the Structure of the "Unstructured" Tau Protein. *Structure.* **2019**, *27*, 1710-1715.
27. Baul, U.; Chakraborty, D.; Mugnai, M.L.; Straub, J.E.; Thirumalai, D. Sequence Effects on Size, Shape, and Structural Heterogeneity in Intrinsically Disordered Proteins. *J Phys Chem B.* **2019**, *123*, 3462-3474.
28. Li, X.; Dong, X.; Wei, G.; Margittai, M.; Nussinov, R.; Ma, B. The Distinct Structural Preferences of Tau Protein Repeat Domains. *Chem Commun (Camb).* **2018**, *54*, 5700-5703.
29. Nguyen, P.H.; Derreumaux, P. Structures of the Intrinsically Disordered Aβ, tau and α-synuclein Proteins in Aqueous Solution from Computer Simulations. *Biophys. Chem.* **2020**, *264,* 106421.
30. Nguyen, P.H.; Tuffery, P.; Derreumaux, P. Dynamics of Amyloid Formation from Simplified Representation to Atomistic Simulations. *Methods Mol Biol.* **2022**, *2405*, 95-113.
31. Stelzl, L.S.; Pietrek, L.M.; Holla, A.; Oroz, J.; Sikora, M.; Köfinger, J.; Schuler, B.; Zweckstetter, M.; Hummer, G. Global Structure of the Intrinsically Disordered Protein Tau Emerges from Its Local Structure. *JACS Au.* **2022**, *2*, 673-686.
32. Dong, X.; Bera, S.; Qiao, Q.; Tang, Y.; Lao, Z.; Luo, Y.; Gazit, E.; Wei, G. Liquid-Liquid Phase Separation of Tau Protein Is Encoded at the Monomeric Level. *J Phys Chem Lett.* **2021***, 12*, 2576-2586.
33. van der Spoel, D.; Lindahl, E.; Hess, B.; Groenhof, G.; Mark, A. E.; Berendsen, H. J. GROMACS: Fast, Flexible, and Free. *J. Comput. Chem.* **2005**, *26*, 1701−1718.
34. Pastor, R.W.; Mackerell, A.D. Jr. Development of the CHARMM Force Field for Lipids. *J Phys Chem Lett.* **2011**, *2*, 1526-1532.
35. Huang, J.; Rauscher, S.; Nawrocki, G.; Ran, T.; Feig, M.; de Groot, B.L.; Grubmüller, H.; MacKerell, A.D. Jr. CHARMM36m: An Improved Force Field for Folded and Intrinsically Disordered Proteins. *Nat. Methods* **2017**, *14*, 71-73.
36. Lee, J.; Cheng, X.; Swails, J.M.; Yeom, M.S.; Eastman, P.K.; Lemkul, J.A.; Wei, S.; Buckner, J.; Jeong, J.C.; Qi; Y. et al. CHARMM-GUI Input Generator for NAMD, GROMACS, AMBER, OpenMM, and CHARMM/OpenMM Simulations Using the CHARMM36 Additive Force Field. *J Chem Theory Comput.* ***2016,*** *12*, 405-413.
37. Bussi, G.; Donadio, D.; Parrinello, M. Canonical Sampling Through Velocity Rescaling. *J Chem Phys.* **2007**, *126*, 014101.
38. Kabsch, W.; Sander, C. Dictionary of Protein Secondary Structure: Pattern Recognition of Hydrogen-bonded and Geometrical Features. *Biopolymers* **1983**, *22*, 2577-2637.

39. Nguyen, T.H.; Nguyen, P.H.; Ngo, S.T.; Derreumaux, P. Effect of Cholesterol Molecules on Aβ1-42 Wild-Type and Mutants Trimers. *Molecules.* **2022,** *27*, 1395.
40. Lu, Y.; Derreumaux, P.; Guo, Z.; Mousseau, N.; Wei, G. Thermodynamics and Dynamics of Amyloid Peptide Oligomerization are Sequence Dependent. *Proteins.* **2009**, *75*, 954-963.
41. Man, V.H.; He, X.; Derreumaux, P.; Ji, B.; Xie, X.Q.; Nguyen, P.H.; Wang, J. Effects of All-Atom Molecular Mechanics Force Fields on Amyloid Peptide Assembly: The Case of $A\beta_{16-22}$ Dimer. *J Chem Theory Comput.* **2019**, *15*, 1440-1452.
42. Nguyen PH, Tarus B, Derreumaux P. Familial Alzheimer A2V Mutation Reduces the Intrinsic Disorder and Completely Changes the Free Energy Landscape of the Aβ1-28 Monomer. *J Phys Chem B.* **2014**, *118*, 501-510.
43. Fatafta, H.; Khaled, M.; Owen, M.C.; Sayyed-Ahmad, A.; Strodel, B. Amyloid-β Peptide Dimers Undergo a Random Coil to β-sheet Transition in the Aqueous Phase but not at the Neuronal Membrane. *Proc Natl Acad Sci U S A.* **2021**, *118*, e2106210118.
44. Tan, J.; Zhang, J.; Luo, Y.; Ye, S. Misfolding of a Human Islet Amyloid Polypeptide at the Lipid Membrane Populates through β-Sheet Conformers without Involving α-Helical Intermediates. *J Am Chem Soc.* **2019,** *141*, 1941-1948.
45. Yao, Q.Q.; Wen, J.; Perrett, S.; Wu, S. Distinct Lipid Membrane-Mediated Pathways of Tau Assembly Revealed by Single-molecule Analysis. *Nanoscale.* **2022**, *14*, 4604-4613.
46. Gellermann, G.P.; Appel, T.R.; Davies, P.; Diekmann, S. Paired Helical Filaments Contain Small Amounts of Cholesterol, Phosphatidylcholine and Sphingolipids. *Biol Chem.* **2006**, *387*, 1267-1274.
47. Chen, D.; Drombosky, K.W.; Hou, Z.; Sari, L.; Kashmer, O.M.; Ryder, B.D.; Perez, V.A.; Woodard, D.R.; Lin, M.M.; Diamond, M.I. et al. Tau local structure shields an amyloid-forming motif and controls aggregation propensity. *Nat Commun.* **2019**, *10*, 2493.
48. Liu, Y.; Ren, B.; Zhang, Y.; Sun, Y.; Chang, Y.; Liang, G.; Xu, L.; Zheng, J. Molecular Simulation Aspects of Amyloid Peptides at Membrane Interface. *Biochim Biophys Acta Biomembr.* **2018,** *1860*, 1906-1916.
49. Nguyen, P. H.; Campanera, J. M.; Ngo, S. T.; Loquet, A.; Derreumaux, P., Tetrameric Aβ40 and Aβ42 β-Barrel Structures by Extensive Atomistic Simulations. I. In Bilayer Mimicking a Neuronal Membrane. *J. Phys. Chem. B* **2019,** *123*, 3643-3648.
50. Doig, A.J.; Del Castillo-Frias, M.P.; Berthoumieu, O.; Tarus, B.; Nasica-Labouze, J.; Sterpone, F.; Nguyen, P.H.; Hooper, N.M.; Faller, P.; Derreumaux, P. Why Is Research on Amyloid-β Failing to Give New Drugs for Alzheimer's Disease? *ACS Chem. Neurosci.* **2017**, *8*, 1435-1437.
51. Seidler, P.M.; Boyer, D.R.; Rodriguez, J.A.; Sawaya, M.R.; Cascio, D.; Murray, K.; Gonen, T.; Eisenberg, D.S. Structure-based Inhibitors of Tau Aggregation. *Nat Chem.* **2018**, *10*, 170 -176.
52. Zheng, Q.; Kebede, M.T.; Kemeh, M.M.; Islam, S.; Lee, B.; Bleck, S.D.; Wurfl, L.A.; Lazo, N.D. Inhibition of the Self-Assembly of Aβ and of Tau by Polyphenols: Mechanistic Studies. *Molecules.* **2019,** *24*, 2316.

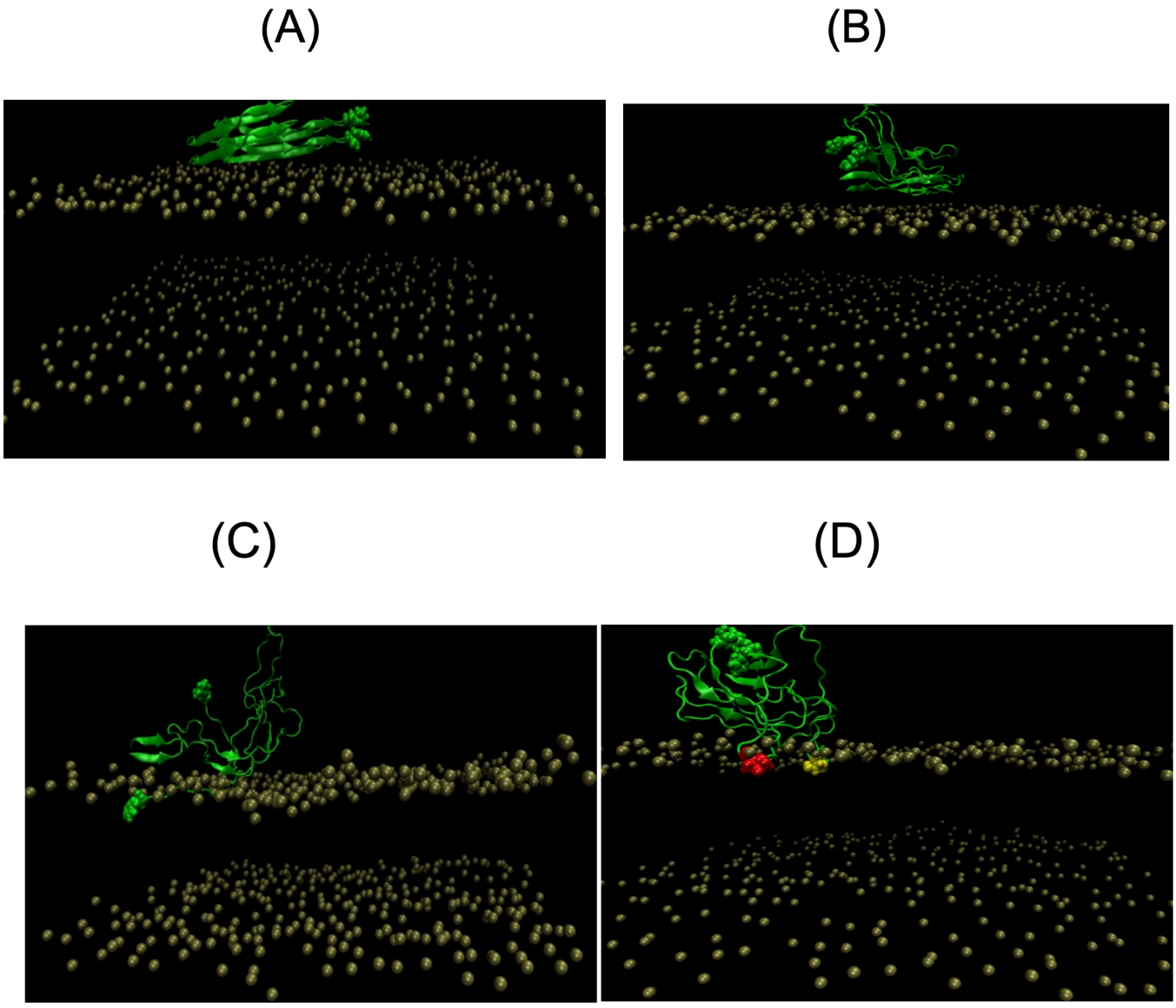

Figure 1. Tau306-378 dimer conformations. In all panels, the phosphate atoms of the lipid heads are in tan, and we show the van der Waals representation of the side-chains of F378 residue in green. (A) Initial cryo-EM structure. (B) Initial globular compact structure. (C) Final structure (2 μs) from the cryo-EM simulation with one F378 side-chain inserted into the membrane and the other exposed to solvent. (D) Final structure from the compact shape simulation, we show the van der Waals representation of two inserted side-chains: S320 in yellow and P364 in red.

(A)

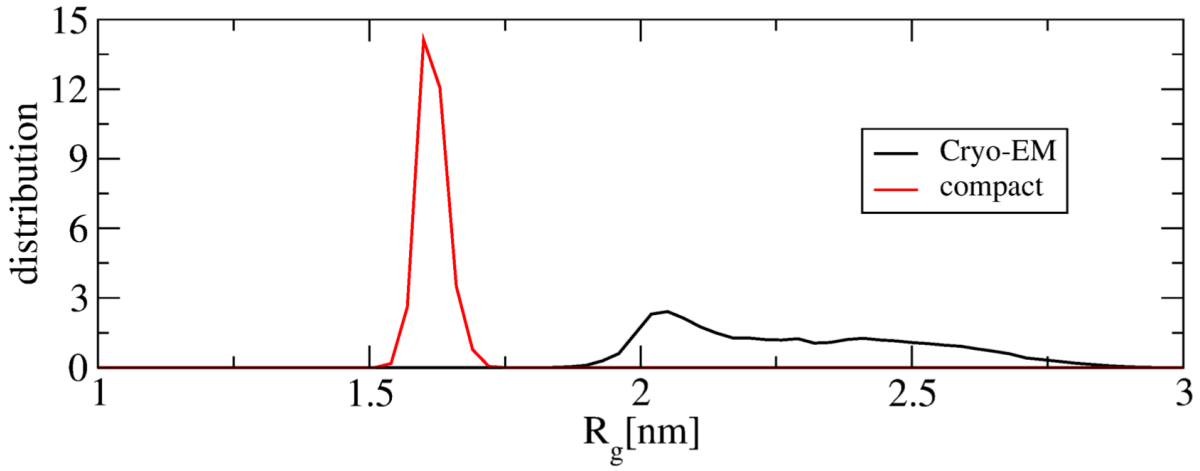

(B)

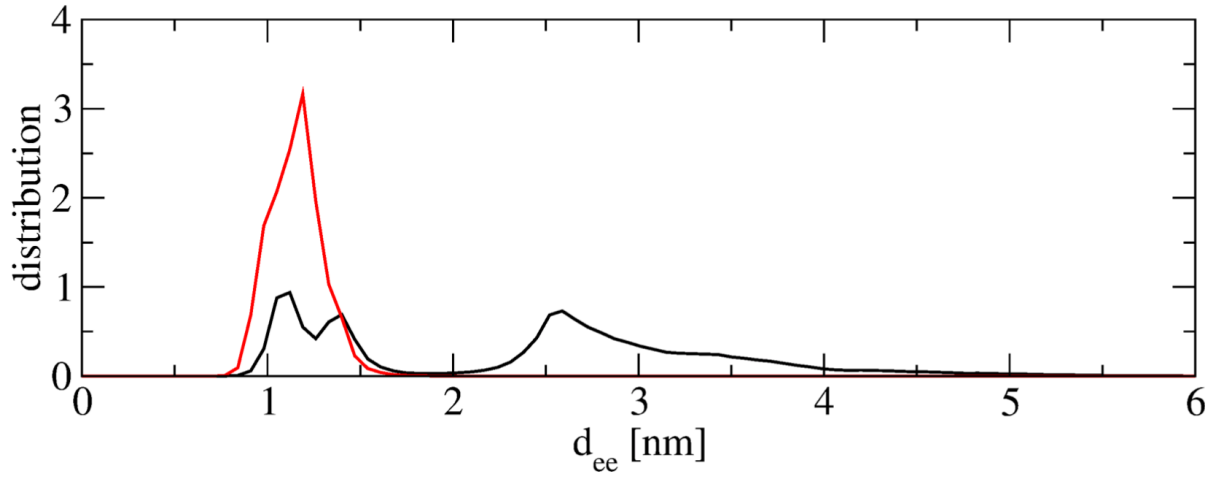

Figure 2. Structural distributions starting from the cryo-EM and compact globular structures. (A) Distributions of Rg values. (B) Distributions of end-to-end distances.

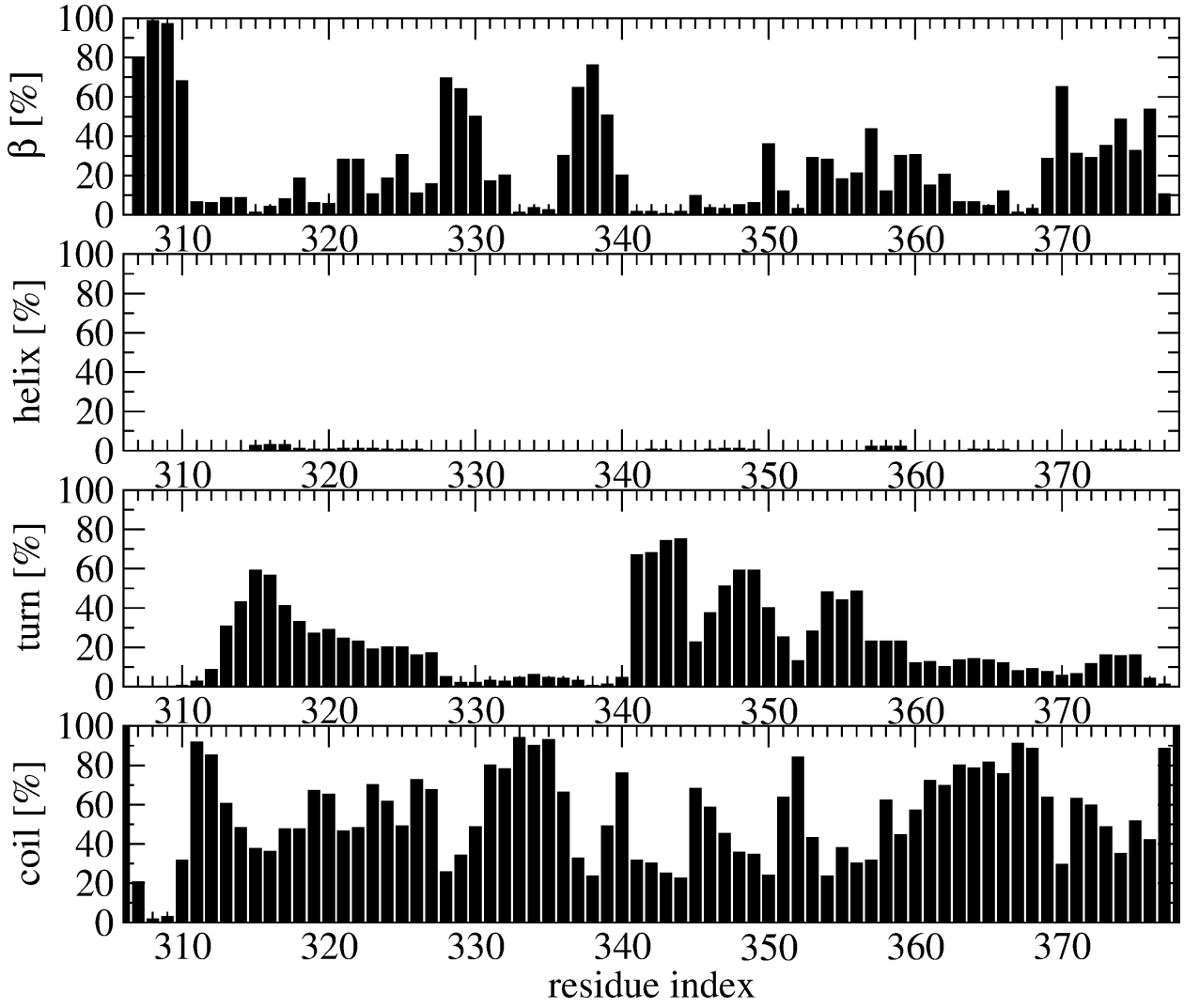

Figure 3. Time-averaged secondary structure contents along the sequence averaged over the two simulations.

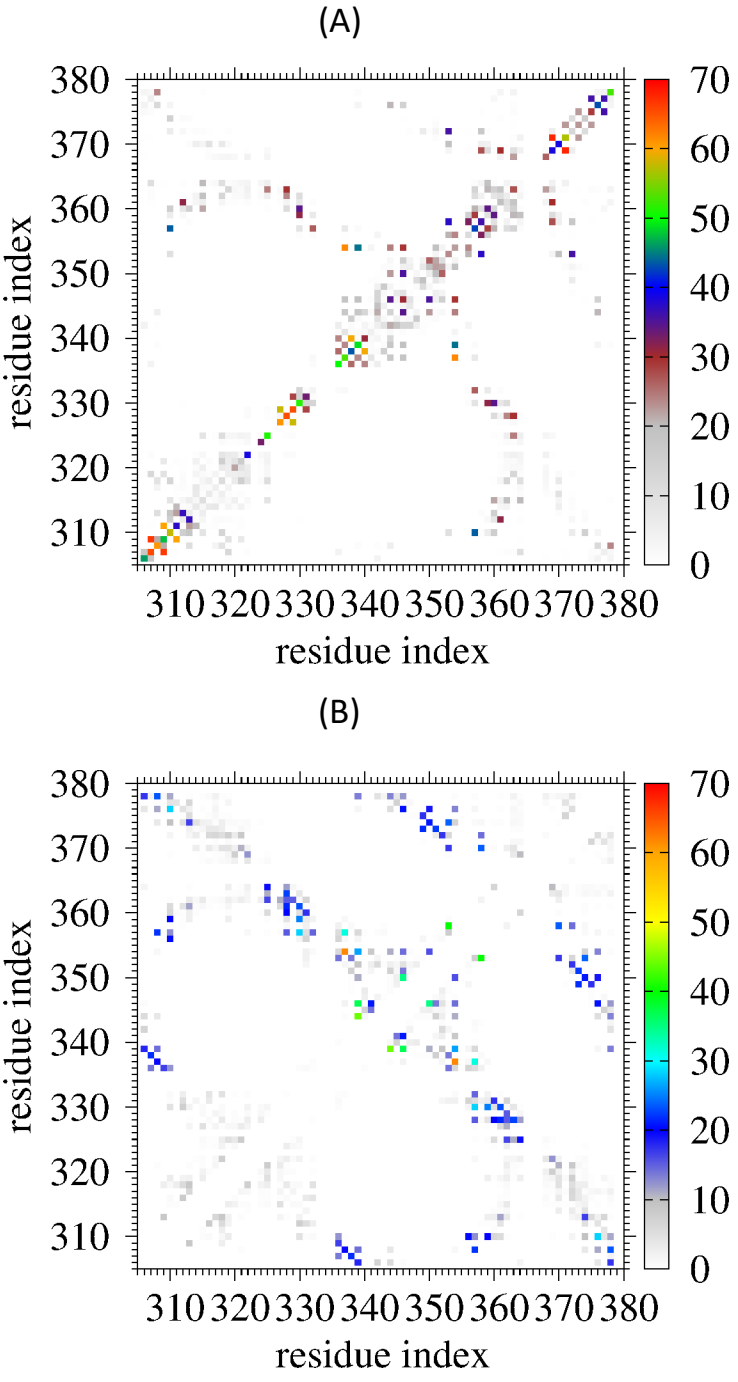

Figure 4. Side-chain contact map probabilities. (A) intermolecular. (B) intramolecular.

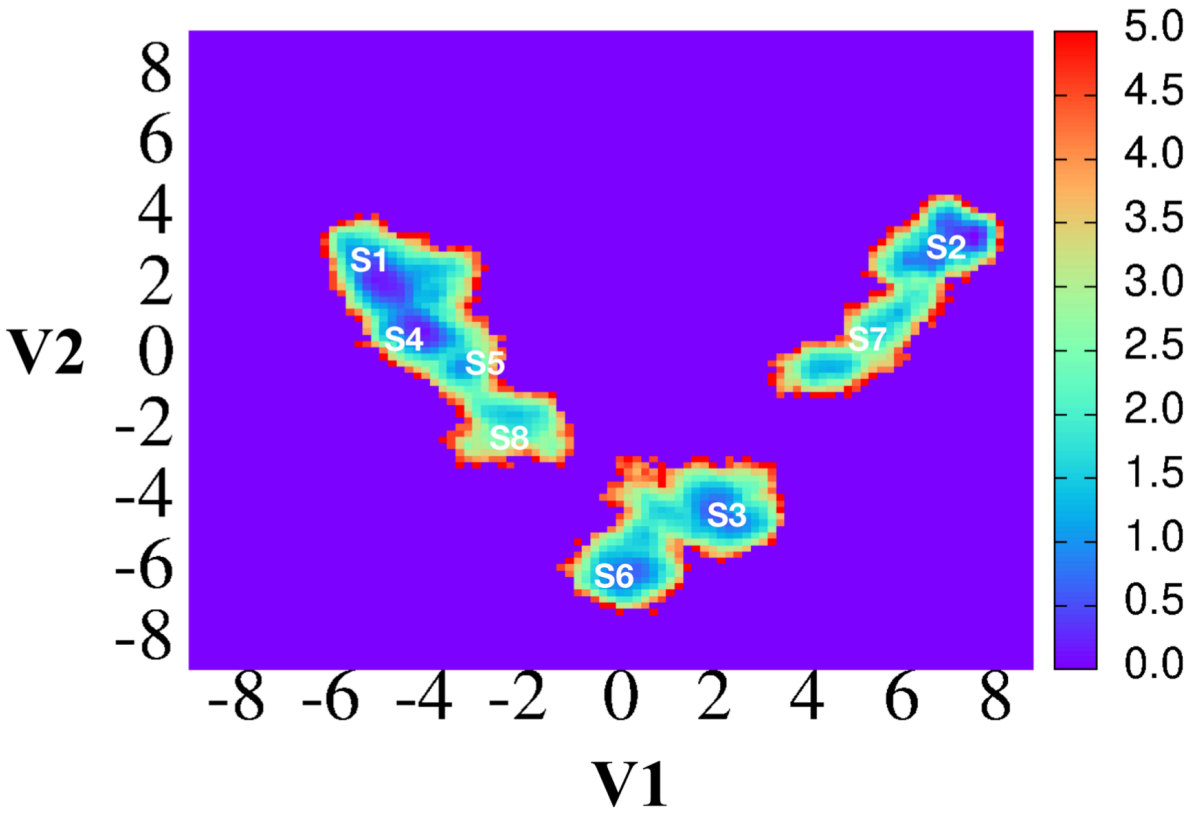

Figure 5. Free energy landscape (in kcal/mol) of tau306-378 dimer and identification of the Si (i=1 to 8) free energy minima.

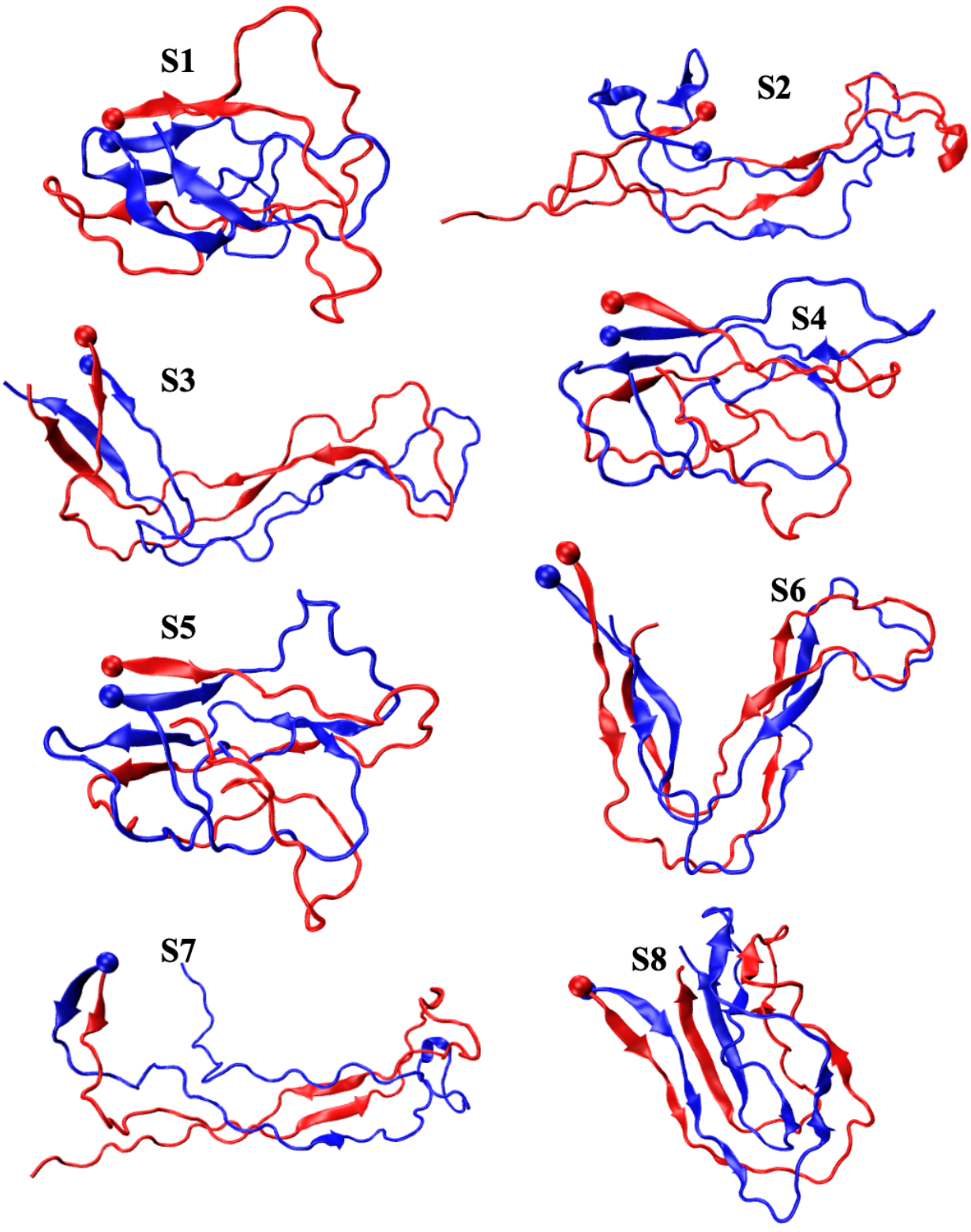

Figure 6. Centers of the eight free energy minima of tau in the membrane simulation. The ball indicates the position of the V306 N-terminus residue.

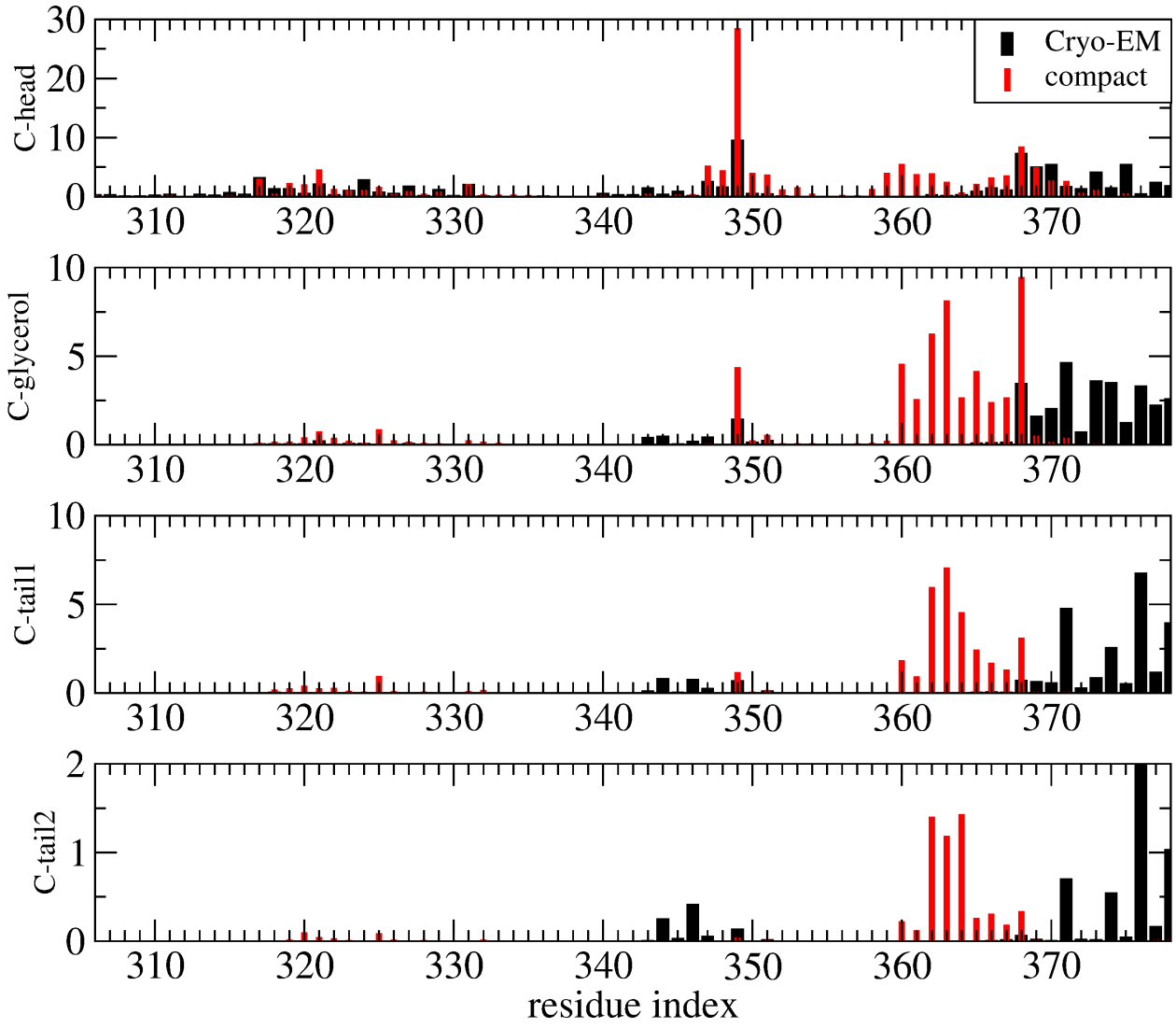

Figure 7. Total number of contact pairs between the side-chain of each residue and each lipid component (head, glycerol, tail1 and tail2) using the full trajectory of each run. Tail2 starts at carbons 21 and 31.

TOC

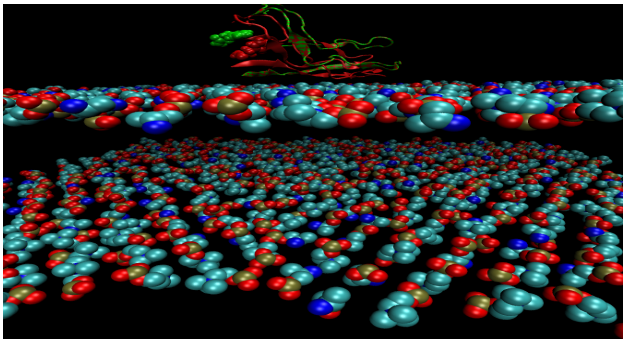

Supporting Information

Molecular Dynamics Simulations of the Tau Amyloid Fibril Core Dimer at the Surface of a Lipid Bilayer Model: I. In Alzheimer's Disease

Phuong H Nguyen,[1] and Philippe Derreumaux [2*]

1 CNRS, Université de Paris, UPR 9080, Laboratoire de Biochimie Théorique, Institut de Biologie Physico-Chimique, Fondation Edmond de Rothschild, 13 rue Pierre et Marie Curie, 75005 Paris, France.

2 Institut Universitaire de France (IUF)

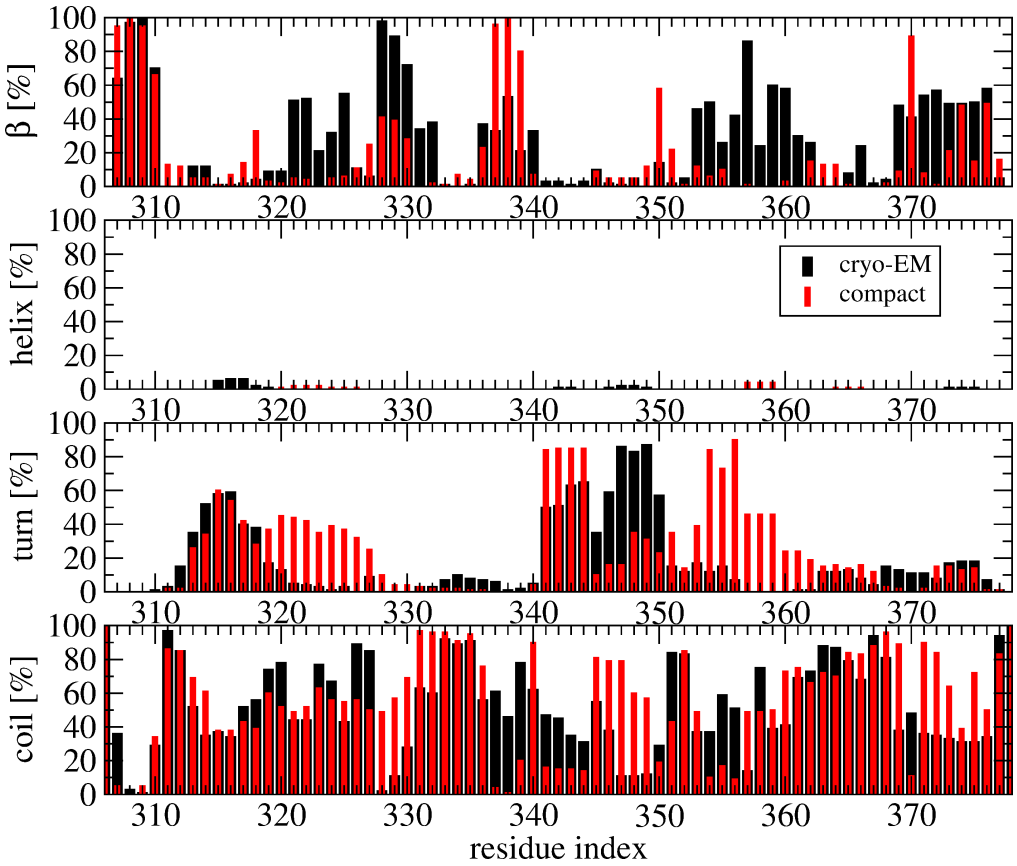

Figure S1. Secondary structure composition along the amino acid sequence starting from the cryo-EM and the compact structures.

State	P [%]	β [%]	Helix [%]	Turn [%]	Coil [%]	Rg [nm]	C
S1	21.41	19.05	0.77	26.83	53.34	1.59	685
S2	20.52	22.76	0.65	20.15	56.42	2.26	634
S3	14.00	33.21	0.50	16.26	50.01	2.52	224
S4	13.91	17.95	0.19	23.65	58.19	1.60	587
S5	11.76	17.59	0.03	21.29	61.07	1.59	481
S6	11.02	34.40	0.00	14.57	51.01	2.23	204
S7	4.46	23.02	0.46	18.49	58.00	2.48	351
S8	2.91	28.39	0.00	18.92	52.67	1.64	96

Table S1. Characterization of the eight clusters identified on the free energy landscape of tau dimer in interaction with a membrane model. For each state, we give the population of the cluster. Also shown are the secondary structure compositions and the Rg values using all conformations belonging to each cluster, as well as the total number of side-chain contacts with the membrane (the sum of C-head, C-glycerol, C-tail1 and C-tail2 contacts).

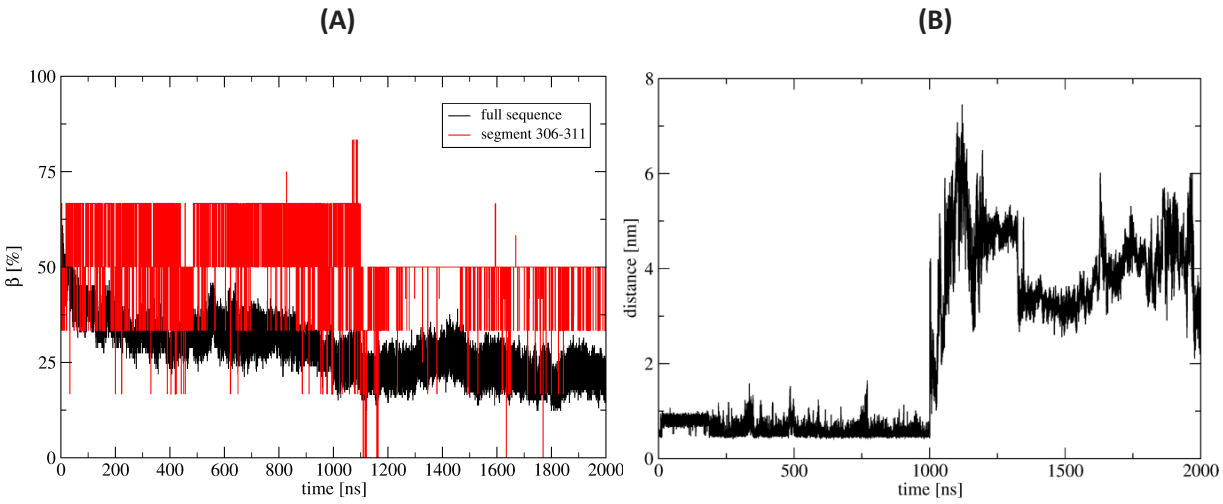

Figure S2. Time-evolution of structural parameters starting from the cryo-EM structure. (A) β-strand character of the PHF6 motif (residues 306-311) and full sequence. (B) Intermolecular Cα F378-F378 distance.

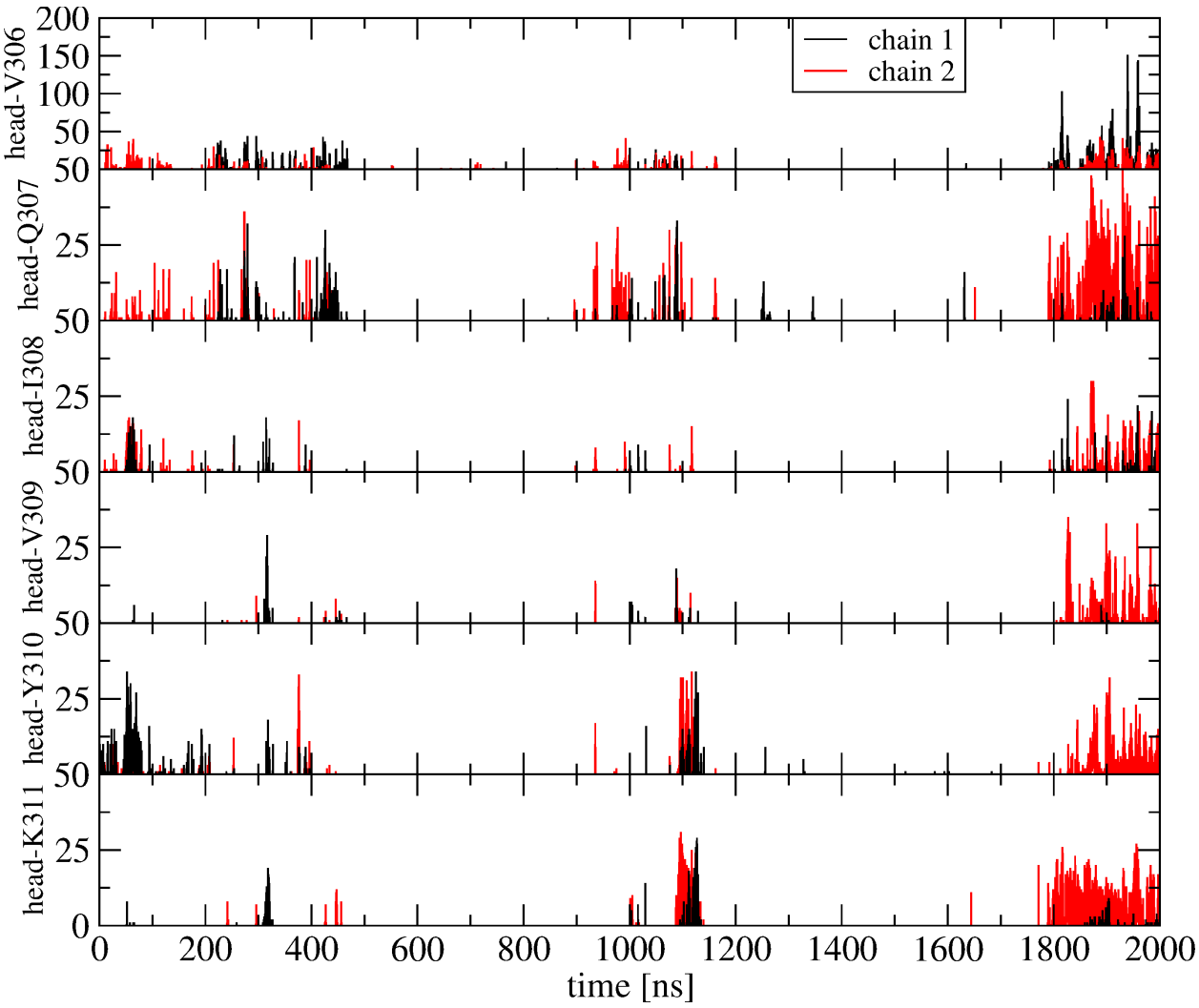

Figure S3. Time-evolution of the total number of contacts between head lipids and each residue of PHF6 including backbone and side-chain heavy atoms starting from the cryo-EM structure.

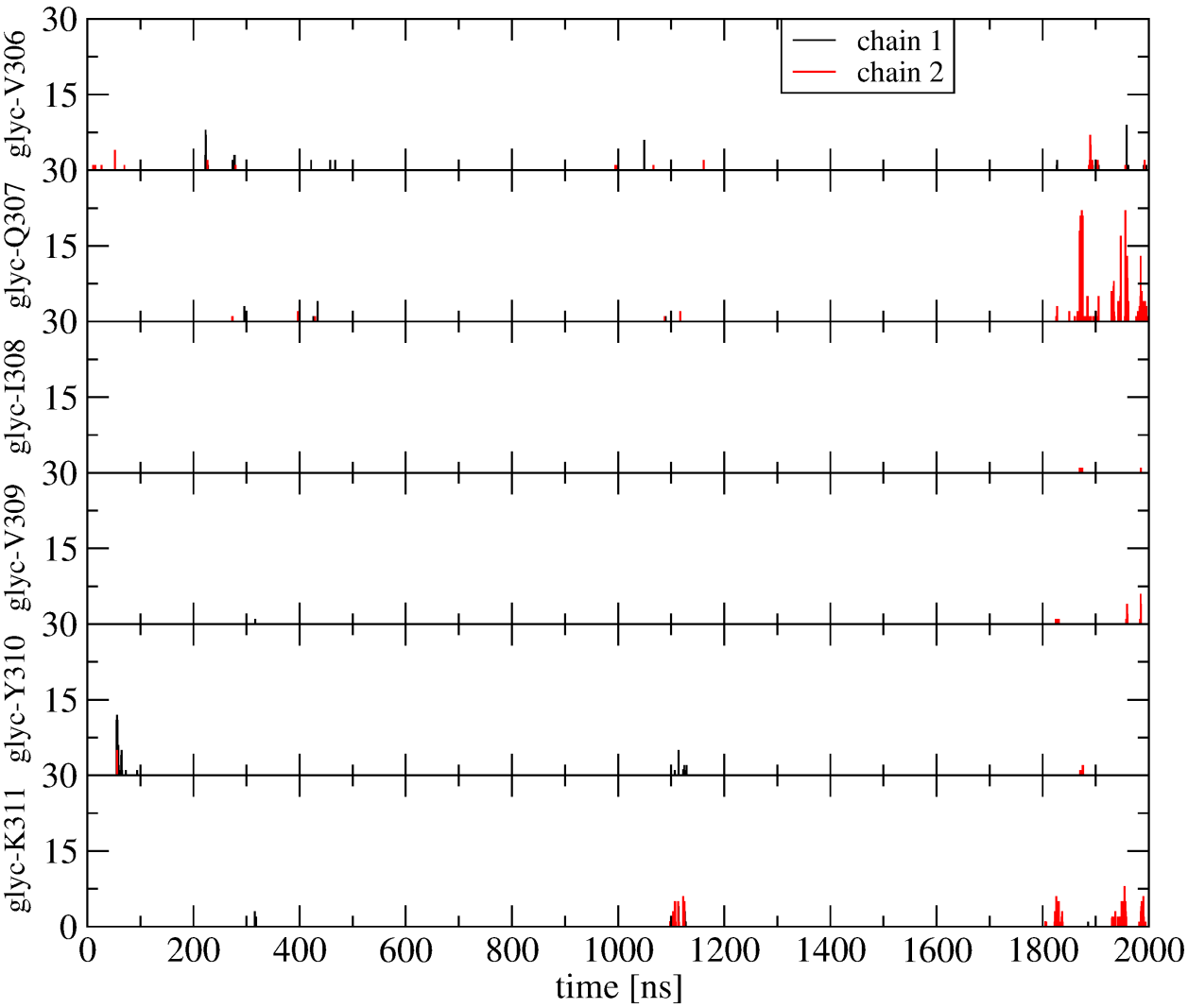

Figure S4. Time-evolution of the total number of contacts between glycerol lipids and each residue of PHF6 including backbone and side-chain heavy atoms starting from the cryo-EM structure.